
REDUCTION OF LASER SELF-FOCUSING IN PLASMA BY POLARIZATION SMOOTHING

*E. Lefebvre**

B. J. MacGowan

R. L. Berger

J. E. Rothenberg

A. B. Langdon

E. A. Williams

Introduction

Achievement of inertial confinement fusion with upcoming megajoule-scale laser facilities requires intense laser light to be propagated through thousands of wavelengths of underdense plasma—a situation naturally susceptible to vigorous growth of laser-plasma instabilities. These instabilities affect the propagation of the incident light by absorbing and/or scattering energy; they prevent efficient coupling to the target and can threaten the symmetry of the x-ray drive imposed on the capsule. The eventual result is a reduction of the safety margin included in the design of the facilities. These detrimental processes are most violent in the so-called hot spots of the beam, where the laser intensity is significantly higher than its average value over the focal spot. Moreover, the concentration of energy into the hot spots is itself prone to an unstable phenomenon, known as self-focusing or filamentation.¹⁻³ In the regions of high laser intensity, the increased thermal electron pressure and the ponderomotive force cooperate to expel the plasma, increasing the refractive index and leading to a still higher intensity. Temporal and spatial smoothing have been observed to significantly reduce both the backscatter⁴⁻⁶ and filamentation⁷ from underdense plasmas. Stimulated Raman and Brillouin backscattering from very low-density plasma, associated with strong filamentation, was virtually eliminated with temporal smoothing.^{5,6} Suppressing filamentation is therefore needed to control backscattering instabilities and requires as much beam smoothing as possible.

A number of approaches to smoothing have been proposed for megajoule-class lasers.⁸⁻¹² One such approach is to use a random phase plate (RPP)⁹ to homogenize the long-scale structure of the focal spot and to then reduce the residual fine-scale speckle

within the focal envelope by using the temporal smoothing by spectral dispersion (SSD) method.¹⁰ In this method, the laser pulse is spectrally broadened by phase modulation, and the resulting bandwidth is then angularly dispersed by a diffraction grating so different frequencies produce shifted speckle patterns that average out in the focal plane. From a time domain viewpoint, the speckle pattern in the focal plane changes at a rate determined by the total bandwidth of the modulation, and thus, the time-integrated intensity seen by the plasma is smoothed. If this rate is more rapid than the plasma hydrodynamic response time, then one expects the smoothing method to be effective in reducing self-focusing. However, this rate is bounded by practical limits on the maximum laser bandwidth, and an alternative or complementary smoothing technique is therefore of great interest.

In this article, we present the first calculations of the effect of polarization smoothing (PS) on the filamentation instability. These calculations show that PS by itself is highly effective in controlling filament formation. In addition, it is shown that PS, with unexpected efficacy, can be combined with SSD to provide suppression greater than either smoothing technique can provide alone. Because PS can be implemented in a large laser system without loss of performance and at reasonable cost, it is a smoothing alternative that satisfies the requirements of both laser engineers and inertial fusion target scientists.

Polarization Smoothing in Vacuum

A few simple techniques have been suggested for PS.¹¹⁻¹³ In the implementation examined here, the laser beam is incident upon a wedged birefringent crystal, with its linear polarization at 45° from both the ordinary and extraordinary axes of the crystal.¹¹ The

*Commissariat à l'Énergie Atomique, Bruyères-le-Châtel, France

crystal output then consists of two beams with equal intensities and orthogonal polarizations. Their directions of propagation are separated by an angle α to the wedge θ ; the birefringence Δn of the crystal: $\alpha = \theta \Delta n$.¹⁴ Due to their orthogonal polarizations, the two waves do not interfere in the target plane, and the total incident intensity is simply the sum of both intensities. The angular shift between the beams in the near-field translates into a spatial shift at focus: $\Delta x = \alpha L = \alpha f D$, where L and f are the focal length and the f -number of the lens, and D is the width of the beam at the lens. The intensity speckle pattern of one beam at focus has a transverse coherence length of $l_{\perp} = f \lambda_0$.^{15,16} For the sum of the two beams, the intensity statistics are determined by the correlation between the shifted speckle patterns,¹⁵ and hence the displacement Δx . The correlation function, $g(\Delta x)$, is given by the Fourier transform of the near-field beam aperture. In our simulations, the beam is square, and $\Delta x = [\sin(\pi \Delta x / f \lambda_0)] / (\pi \Delta x / f \lambda_0)$. It is straightforward to determine the intensity distribution function for a finite displacement, x , between the patterns. The probability $P(I) dI$ that the total intensity lies in the interval, I to $I + dI$, is given by

$$P(I) = \frac{4I}{I_0^2(1-g^2)} \exp\left[\frac{-2I}{I_0(1-g^2)}\right] \int_0^1 ds I_0 \left(\frac{gI\sqrt{1-s^2}}{I_0(1-g^2)}\right). \quad (1)$$

The function I_0 is the modified Bessel function of zeroth order. If the separation between the two beams is much smaller than the transverse coherence length of one of them, $\Delta x \ll l_{\perp}$, the intensity statistics in vacuum have the exponential distribution of a single beam; the probability $P_1(I) dI$ that the total intensity lies in the interval, I to $I + dI$, is given by $P_1(I) = \exp(-I/I_0)/I_0$, where I_0 is the total average intensity.¹⁵ An elementary calculation then shows that the fraction of beam energy contained in regions where the intensity is higher than nI_0 is $F_1(n) = (1+n)\exp(-n)$. Hence, e.g., 4% of the beam energy has a local intensity above $5I_0$. Conversely, if the beams are completely uncorrelated (e.g., a displacement of $f\lambda_0$), $g = 0$, and the intensity distribution is that of the incoherent sum of two speckle patterns governed by $P_2(I) = 4I \exp(-2I/I_0)/I_0^2$. Now the fraction of beam energy above nI_0 reads $F_2(n) = (1+2n+2n^2)\exp(-2n)$, and is less than 0.3% for $n = 5$. The intensity contrast, defined as

$$\sigma = \sqrt{\frac{\langle I^2 \rangle}{I_0^2} - 1},$$

is reduced from 1 for one RPP beam to $1/\sqrt{2}$ for the superposition of two uncorrelated beams,¹⁵ indicating a smoother intensity distribution.

Polarization Smoothing in a Plasma

These promising properties of speckle statistics in vacuum will be modified in a plasma, where the electron density, and hence the refractive index, is nonlinearly dependent on the local intensity. To model this intricate laser-plasma coupling, we used the code F3D, which has been described elsewhere.³ For this first study, we limited our attention to the “slow” ion waves responsible for self-focusing and filamentation of the light. PS is modeled by generating two tilted beams at the final focusing lens, resulting in two shifted speckle patterns in the focal plane. To advance the simulation by one time step, each beam is propagated independently (in the z direction) in the density profile. The total intensity distribution in the plasma is then computed by summing the intensities of both beams, and it is used to update the plasma hydrodynamic quantities (density, momentum, and energy) through the ponderomotive and thermal pressures.

The parameters that we used in our simulations are representative of the plasmas that will be produced inside the hohlraums of the future megajoule-scale lasers:⁶ equimolar CH mixture; electron density $n_e = 0.1n_c$, where n_c is the critical density at the laser wavelength $\lambda_0 = 0.35 \mu\text{m}$; and electron and ion temperatures $T_e = 3 \text{ keV}$ and $T_i = 1 \text{ keV}$, respectively. The incident light is focused with an $f/8$ square lens. Unless otherwise specified, the laser intensity is $I_0 = 2 \times 10^{15} \text{ W/cm}^2$. The plasma is typically two speckle lengths long, i.e., $2l_{\parallel} = 16f^2\lambda_0 = 1024\lambda_0$, and the usual simulation time is 100 ps. SSD is modeled in its simplest form (1D-SSD),¹⁰ where the laser is sinusoidally phase modulated (FM) at a modulation frequency ν_{FM} , and the grating dispersion is chosen such that the FM sidebands are each separated at focus by $f\lambda_0$ in the y direction (“critical dispersion”).

Results and Discussion

Filamentation in the plasma can dramatically change the intensity distribution by increasing the probability of power at high intensity. To illustrate that process and the effect of PS, we display in Figure 1, as a function of position along the propagation axis, the fraction of beam power exceeding five times the average intensity I_0 . This measure of the modified intensity distribution, hereafter called the “tail fraction,” is admittedly arbitrary, but other measures are similar in behavior. Four different smoothing configurations are considered in Figure 1: (a) a beam smoothed by RPP only, (b) a beam smoothed by RPP and SSD along the y direction, (c) a beam smoothed by RPP and PS, with a separation between the two shifted beams $\Delta x = l_{\perp} = 8\lambda_0$

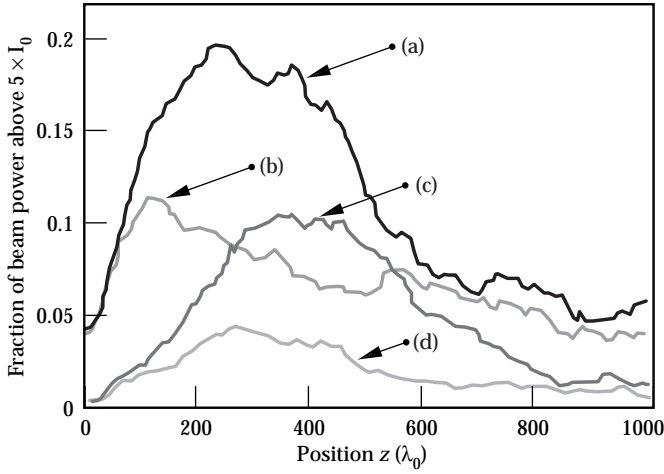


FIGURE 1. Fraction of beam energy above $5I_0$ vs axial position z in the plasma. Smoothing with (a) RPP only; (b) RPP and 1D-SSD (bandwidth $\Delta v/v = 2.5 \times 10^{-4}$, $v_{FM} = 20$ GHz); (c) RPP and PS (beams shifted by $f\lambda_0$ in the target plane); (d) RPP, 1D-SSD and PS as above, with orthogonal dispersions. (50-00-0898-1678pb01)

along x , and finally (d) a beam smoothed by a conjunction of all three techniques (RPP, SSD along y , and PS along x). For all cases the tail fraction first increases monotonically with distance, as small filaments form in the target, concentrating large amounts of the incident energy to high irradiance. Then the tail fraction drops back to roughly its initial value, indicating that the small filamented structures defocus. The first two curves, without PS, start at the value of 4% expected for irradiation by a single beam. Whereas curve (a) reaches a maximum of $\sim 20\%$, curve (b) grows at the same rate but stops at 11%. SSD apparently has little effect on the focusing of the most unstable hot spots, but is effective in stabilizing the more slowly growing filaments. The PS case, curve (c) starts from a lower value and increases more slowly in space, which reflects the lack of power in fast-growing filaments. That is, PS reduces the power at high intensity in the incident beam. It even turns out, in this case, that the maximum tail fraction is slightly lower than that produced by SSD. Finally [curve (d)], using both techniques is highly effective because PS eliminates the power in fast-growing filaments, while SSD suppresses the growth of slower filaments. The maximum tail fraction in this last case is about the same (4%) as that for an RPP beam in vacuum, illustrating the effectiveness of PS.

The time history of the tail fractions (measured, at each time, at the z positions where their maxima are achieved) confirms the above description, even though the maximum tail fraction can oscillate in time by a few percent around the values of Figure 1. The rise time with PS is slightly longer than with the RPP alone (10 ps versus 7 ps), whereas the growth with SSD is much slower (rise time ~ 50 ps) and oscillatory. The

maximum intensity in the plasma reaches $50I_0$ when only an RPP is used, but is limited to $14I_0$ when PS and SSD are operated together. The values for SSD alone and PS alone are similar, around $30I_0$.

The importance of using SSD and PS together can be illustrated more practically. For a beam smoothed by RPP only, roughly 21% of the energy will be above $5I_0 = 10^{16}$ W/cm² at maximum. If we use an SSD- and PS-smoothed beam with the parameters mentioned above and tolerate the same fraction of beam energy above 10^{16} W/cm², we can use a pulse with nearly twice the average intensity: $I_0 = 4 \times 10^{15}$ W/cm². On the other hand, if we only accept the same absolute amount of energy above 10^{16} W/cm², we can still drive the plasma around $I_0 = 3 \times 10^{15}$ W/cm², i.e., at a 50% higher intensity with RPP, SSD, and PS than with RPP alone.

From another point of view, PS can effectively increase the bandwidth of the pulse, but without the usual decrease in laser performance. In fact, at $I_0 = 2 \times 10^{15}$ W/cm², the benefit provided by PS seems out of reach of SSD alone, as shown in Figure 2. When the pulse bandwidth is increased from $\Delta v/v = 2.5 \times 10^{-4}$ to 6×10^{-4} , the tail fraction produced by a SSD-smoothed beam only drops from 13% to 10%, far from the 5% obtained with PS at $\Delta v/v = 2.5 \times 10^{-4}$. The same conclusion holds at $I_0 = 4 \times 10^{15}$ W/cm², where a bandwidth $\Delta v/v = 6 \times 10^{-4}$ results in a maximum tail fraction of roughly 15%, whereas it is only 9% to 10% for a combined smoothing by SSD ($\Delta v/v = 2.5 \times 10^{-4}$ at 3 GHz) and PS ($\Delta x = f\lambda_0$). Figure 2 also confirms the effectiveness of PS alone relative to SSD alone. With PS alone, the tail fraction is found to be $\sim 12\%$. To achieve an

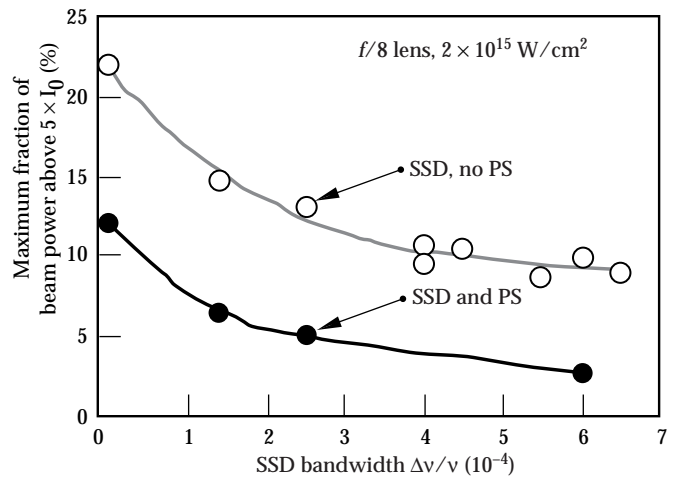


FIGURE 2. Maximum value along z for the fraction of beam energy above $5I_0$, averaged over the last 20 ps of the simulation, vs bandwidth of the 1D-SSD, with or without PS ($\Delta x = f\lambda_0$). Different v_{FM} guides have been used. (The solid lines are fits to guide the eye.) (50-00-0898-1679pb01)

equivalent tail fraction with SSD alone requires a bandwidth of $\Delta\nu/\nu \sim 3 \times 10^{-4}$. This result is quite notable in that PS only sums two speckle patterns, whereas SSD (asymptotically) sums many more; at $\Delta\nu/\nu = 3 \times 10^{-4}$ and $\nu_{\text{FM}} = 3$ GHz, the number of FM sidebands, and hence speckle patterns, is ~ 85 . This emphasizes the importance of the instantaneous nature of PS, and one can conclude that the temporal smoothing rate is critical for suppression of filamentation.

It is interesting to note that some of the data points in Figure 2 have been obtained with 3 GHz SSD, and the other ones with 20 GHz SSD, in both cases critically dispersed. Yet both series obviously lie on the same curve. At a fixed bandwidth $\Delta\nu$, a change in the SSD modulation frequency does not change the time it takes for two independent speckle patterns to be successively generated in the focal plane, which is simply the coherence time, $\tau = 1/\Delta\nu$. Yet a higher SSD modulator frequency means that fewer independent speckle patterns will be formed on the target, so that the asymptotic contrast value will be higher (meaning less smoothing) and reached in a shorter time. The insensitivity of the plasma to the modulation frequency is explained by the fact that its reaction time is of the order of the laser coherence time, so that the larger number of speckle patterns produced in the low ν_{FM} case appears well after the plasma has responded and cannot effectively participate in smoothing the intensity distribution. This is fully consistent with the above statement that the instantaneous smoothing produced by PS is paramount to explaining its effectiveness. Moreover, this also supports using a relatively high SSD modulation frequency in future facilities, since a critically dispersed beam is less divergent at high ν_{FM} . Then the usual difficulties of propagating a divergent beam through a laser chain (such as pinhole clipping in the spatial filters, modification of the pulse shape, and smearing of the focal spot) can be substantially reduced, without negatively impacting the smoothing efficiency.

As is the case in vacuum, the efficiency of PS depends on the amount of spatial separation that is introduced between the beams in the target plane. Our results for $I_0 = 1, 2$ and 4×10^{15} W/cm² are summarized in Figure 3. The conditions for these simulations are an RPP only (open points); or an RPP, SSD along y with $\nu_{\text{FM}} = 3$ GHz and bandwidth $\Delta\nu/\nu = 2.5 \times 10^{-4}$ (closed points); and PS with a variable shift along x between the two beams (shaded points). Linear optics in vacuum (see ‘‘Polarization Smoothing in Vacuum’’ on p. 83) suggests that the absolute minimum in the tail fraction should be reached for a shift equal to $\Delta x = f\lambda_0$. Plasma-induced nonlinearities modify this simple picture, and the tail fraction appears to be best minimized only for shifts $\geq 2f\lambda_0$.

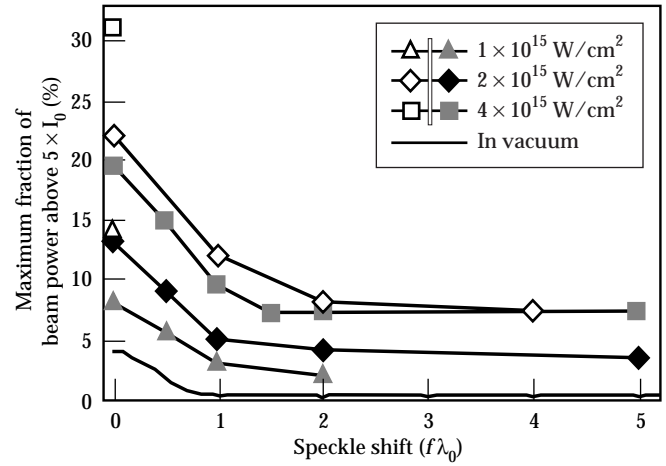


FIGURE 3. Maximum value along z for the fraction of beam energy above $5I_0$, averaged over the last 20 ps of the simulation, vs beam separation at focus. The open symbols correspond to RPP only, the closed ones to RPP and 1D-SSD ($\nu_{\text{FM}} = 3$ GHz, bandwidth $\Delta\nu/\nu = 2.5 \times 10^{-4}$). Results with zero beam separation are identical to results without PS. The level obtained in vacuum is also plotted. (50-00-0898-1680pb01)

The initial independence between the beam profiles can change as they propagate into the plasma. To assess this effect, we define a normalized cross-correlation function between the intensities I_1 and I_2 of beams 1 and 2 as

$$K(x, y, z) = \frac{\iint dudv [I_1(u, v) - \langle I_1 \rangle][I_2(u - x, v - y) - \langle I_2 \rangle]}{\sqrt{\langle I_1^2 \rangle - \langle I_1 \rangle^2} \times \sqrt{\langle I_2^2 \rangle - \langle I_2 \rangle^2}} \quad (2)$$

where the z dependence of I_1 and I_2 is omitted for clarity, and the brackets stand for averaging over the transverse coordinates u and v . Close to the laser entrance plane and as we expected, the cross-correlation function is maximum and equal to 1 for (x, y) equal to the displacement of beam 1 relative to beam 2. Far from this peak, K typically oscillates around ± 0.1 , owing to the sampling statistics of our finite grid size. We observe two opposing trends when the beams propagate deeper into the plasma— K gets smoothed out, and its maximum oscillates around a low value, $K_{\text{max}} = 0.1$ to 0.2 , but also the location of this maximum can shift toward the origin in the (x, y) plane. The latter observation means that the beams tend to recorelate under the influence of the plasma, each one being focused into the density troughs created by the other. Fortunately, the decay of K is faster than this mutual

attraction—only a small fraction of the beams will effectively be recorrelated, while on the whole, they will even lose the “preferred” cross-correlation distance ($-\Delta x$) that they had at the plasma entrance.

For our nominal conditions, with an initial beam shift $\Delta x = 2f\lambda_0$ and a laser irradiance $I_0 = 2 \times 10^{14}$ W/cm², this decay of the cross-correlation function occurs after propagation through roughly $750 \lambda_0$. When the irradiance is twice as large, it happens after only $375 \lambda_0$. This I^{-1} scaling is consistent with a phenomenon driven by the ponderomotive force of the laser via the plasma density modulations. The variations of K_{\max} with z are established in less than 20 ps and remain constant in time thereafter. If the initial separation between the beams, or their intensity, is varied, the competition between recorrelation and decorrelation can evolve differently. At $I_0 = 4 \times 10^{15}$ W/cm², e.g., the decay of K along the z axis is roughly the same for $\Delta x = 2f\lambda_0$ and $\Delta x = 1f\lambda_0$, but the maximum of K is localized around the origin in the latter case, indicating less decorrelation by the plasma. When the shift is reduced further to $\Delta x = 0.5f\lambda_0$, K steadily maximizes at the origin of the (x, y) plane after propagation along $400 \lambda_0$, with a value of 0.5, supporting a stronger but still partial recorrelation of the beams. This cross-influence of the beams explains why it can be more effective, contrary to what linear optics suggests, but in agreement with Figure 3, to use an initial separation Δx greater than $I_{\perp} = f\lambda_0$. Note that other implementations of PS,^{12,13} where the second beam is completely decorrelated from the first one instead of simply being a shifted duplicate, can significantly reduce this concern. This is, for instance, the case if the orthogonally polarized pulses are transmitted through different phase plates.

Because PS and SSD each disperse in a selected direction, one expects different results depending on whether the PS dispersion is parallel or orthogonal to the direction of SSD dispersion. SSD can be thought of as generating on target a large number of speckle patterns shifted along y . If the PS dispersion is in the same direction, we might expect only a small benefit since the additional dispersion is only marginal. On the other hand, if PS shifts the beams in the orthogonal (x) direction, the maximum smoothing is expected. This effect is simulated with the same plasma parameters as above, SSD bandwidth of $\Delta v/v = 2.5 \times 10^{-4}$, $v_{\text{FM}} = 30$ GHz, a shift of $2f\lambda_0$ between the PS-generated beams, and a simulation time of 110 ps. For an average intensity $I_0 = 10^{15}$ W/cm², the tail fraction averages to 2% if PS is dispersed along x and 3% if it is dispersed along y parallel to SSD. At $I_0 = 2 \times 10^{15}$ W/cm², the tail fractions for the two directions are still similar—3.5% for PS orthogonal to SSD and 5% for PS parallel to

SSD, both much smaller than the 13% obtained without PS. Thus, one sees that PS is quite effective even when it is applied along the same direction as SSD. This is due to the fact that even though the PS dispersion is small compared to SSD, PS acts instantaneously, whereas SSD irradiates the plasma with a speckle pattern that changes at the bandwidth limited rate. The addition of PS reduces the tail fraction by smoothing the changing speckle pattern at each instant in time. Although not simulated here, our results suggest that similar benefits will be obtained when PS is combined with any other temporal smoothing method, such as the induced spatial incoherence method.⁸

Conclusion

In conclusion, we have investigated the dynamics of an underdense plasma, typical of those that will be produced by next-generation megajoule-class lasers, when irradiated by an intense laser whose intensity speckle inhomogeneities are reduced by polarization smoothing. The essence of this scheme lies in the superposition, in the focal plane, of two orthogonally polarized and uncorrelated speckle patterns, that, e.g., can be achieved with a wedged birefringent crystal. For intensities of a few times 10^{15} W/cm², polarization smoothing was found to be highly effective in reducing the self-focusing of light in the plasma. Its operation in conjunction with SSD leads to a suppression of self-focusing that could not be achieved by SSD alone. We found that a relatively small shift (typically $2f\lambda_0$) between the orthogonally polarized beams in the focal plane is sufficient to achieve this result, since the tendency of the beams to recorrelate as they propagate is found to be limited.

Acknowledgments

The authors acknowledge valuable discussions with G. Bonnaud, T. W. Johnston, and C. H. Still. This work was a cooperation in High-Energy Laser-Matter Interaction Physics by the Commissariat à l'Énergie Atomique and the U.S. Department of Energy.

Notes and References

1. P. Kaw, G. Schmidt, and T. Wilcox, *Phys. Fluids* **16**, 1522 (1973); F. W. Perkins and E. J. Valeo, *Phys. Rev. Lett.* **32**, 1234 (1974).
2. A. J. Schmitt, *Phys. Fluids* **31**, 3079 (1988); A. J. Schmitt, *Phys. Fluids B* **3**, 186 (1991); H. A. Rose and D. F. DuBois, *Phys. Fluids B* **4**, 252 (1992).
3. R. L. Berger et al., *Phys. Fluids B* **5**, 2243 (1993); C. H. Still, R. L. Berger, A. B. Langdon, and E. A. Williams, *ICF Quarterly Report* **6** (4), 138, Lawrence Livermore National Laboratory, Livermore, CA, UCRL-LR-105821-9G-4 (1996).

4. S. P. Obenschain et al., *Phys. Rev. Lett.* **62**, 768 (1989); W. Seka et al., *Phys. Fluids B* **4**, 2232 (1992); A. N. Mostovych et al., *Phys. Rev. Lett.* **59**, 1193 (1987).
5. J. D. Moody et al., *Phys. Plasmas* **2**, 4285 (1995); D. S. Montgomery et al., *Phys. Plasmas* **3**, 1728 (1996).
6. B. J. MacGowan et al., *Phys. Plasmas* **3**, 2029 (1996).
7. C. Labaune et al., *Phys. Fluids B* **4**, 2224 (1992).
8. R. H. Lehmberg and S. P. Obenschain, *Optics Commun.* **46**, 27 (1983); R. H. Lehmberg and J. Goldhar, *Fusion Technology* **11**, 532 (1987).
9. Y. Kato et al., *Phys. Rev. Lett.* **53**, 1057 (1984).
10. S. Skupsky et al., *J. Appl. Phys.* **66**, 3456 (1989).
11. "Phase conversion using distributed polarization rotation," *LLE Review* **45**, 1 (1990).
12. K. Tsubakimoto et al., *Optics Commun.* **91**, 9 (1992); K. Tsubakimoto et al., *Optics Commun.* **103**, 185 (1993).
13. S. Pau, S. N. Dixit, and D. Eimerl, *J. Opt. Soc. Am. B*, **11**, 1498 (1994).
14. S. G. Lipson, H. Lipson, and D. S. Tannhauser, *Optical Physics*, 3rd ed. (Cambridge University Press, Cambridge, 1995).
15. J. W. Goodman, "Statistical properties of speckle patterns," in *Laser Speckle and Related Phenomena*, edited by J. C. Dainty, (Springer, New York, 1984).
16. The transverse coherence length for a speckle pattern is $l_{\perp} = \ell_{\lambda_0}$ for square laser beams, as modeled here, and $l_{\perp} = 1.22\ell_{\lambda_0}$ for circular ones.